Atmos. Meas. Tech., 5, 123–139, 2012
www.atmos-meas-tech.net/5/123/2012/
doi:10.5194/amt-5-123-2012

Atmospheric Measurement Techniques

Antarctic ozone hole as observed by IASI/MetOp for 2008–2010

C. Scannell[1], D. Hurtmans[2], A. Boynard[1,*], J. Hadji-Lazaro[1], M. George[1], A. Delcloo[3,], O. Tuinder[4], P.-F. Coheur[2], and C. Clerbaux[1,2]**

[1]UPMC Univ. Paris 06; UMR8190, Université Versailles St.-Quentin; CNRS/INSU, LATMOS-IPSL, Paris, France
[2]Spectroscopie de l'Atmosphère, Chimie Quantique et Photophysique, Université Libre de Bruxelles (ULB), Brussels, Belgium
[3]Royal Meteorological Institute of Belgium, Uccle, Belgium
[4]Royal Netherlands Meteorological Institute (KNMI), De Bilt, The Netherlands
[*]now at: Atmospheric Chemistry Division, National Center for Atmospheric Research, Boulder, CO, USA
[**]also at: Department of Sustainable Organic Chemistry and Technology, Faculty of Bioscience Engineering, Ghent University, Ghent, Belgium

Correspondence to: C. Scannell (claire.scannell@gmail.com)

Received: 23 May 2011 – Published in Atmos. Meas. Tech. Discuss.: 22 July 2011
Revised: 7 December 2011 – Accepted: 17 December 2011 – Published: 12 January 2012

Abstract. In this paper we present a study of the ozone hole as observed by the Infrared Atmospheric Sounding Interferometer (IASI) on-board the MetOp-A European satellite platform from the beginning of data dissemination, August 2008, to the end of December 2010. Here we demonstrate IASI's ability to capture the seasonal characteristics of the ozone hole, in particular during polar night. We compare IASI ozone total columns and vertical profiles with those of the Global Ozone Monitoring Experiment 2 (GOME-2, also on-board MetOp-A) and electrochemical concentration cell (ECC) ozone sonde measurements. Total ozone column from IASI and GOME-2 were found to be in excellent agreement for this region with a correlation coefficient of 0.97, for September, October and November 2009. On average IASI exhibits a positive bias of approximately 7 % compared to the GOME-2 measurements over the entire ozone hole period. Comparisons between IASI and ozone sonde measurements were also found to be in good agreement with the difference between both ozone profile measurements being less than ±30 % over the altitude range of 0–40 km. The vertical structure of the ozone profile inside the ozone hole is captured remarkably well by IASI.

1 Introduction

Global monitoring of ozone (O_3) is essential as it plays an important role in the chemical processes occurring in the atmosphere and has a major impact on the climate. In the troposphere ozone is considered to be one of the primary air pollutants and main greenhouse gases and in high pollution areas it has been shown to have significant negative impacts on human health and local ecosystems (Slaper et al., 1996). In the stratosphere however, where ozone concentrations greatly exceed those of the troposphere, ozone works to protect the Earth by absorbing the sun's harmful ultraviolet (UV) radiation.

Since the mid 1980s a noticeable depletion of stratospheric ozone has been observed annually over the Antarctic region during polar spring (August, September, October and November). Annual ozone concentrations of less than 100 DU (Dobson Units) have been recorded during this time. Studies have established that during this period the ozone hole extends over a large part of the Antarctic region and increases the level of UV radiation reaching the Earth's surface in the ozone hole region (Newman et al., 2007). This in turn leads to adverse impacts on human health in parts of South America (de Laat et al., 2010; Slaper et al., 1996).

Ozone loss rates are determined by the concentrations of active chlorine, bromine, nitrogen and hydrogen oxides

present in the atmosphere. It is thought that inside the polar vortex approximately 60 % of the ozone destruction is caused by the release of active chlorine and the remainder by the release of bromine, hydrogen and nitrogen (Feng et al., 2005, 2011). During polar night a polar vortex forms over Antarctic, holding the air mass within. The lack of sunlight leads to reduced temperatures in the lower stratosphere. When temperatures below 195 K and 188 K are reached, type 1 and type 2 polar stratospheric clouds (PSCs) can form (Maturilli et al., 2005). Heterogeneous reactions can take place on the surface of PSCs resulting in the release of active chlorine which is a key element in the catalytic destruction of ozone over the Antarctic when the sun comes back. Furthermore nitric acid (HNO_3), a by-product of the heterogeneous reactions remains within the PSCs, which are lost from the stratosphere via sedimentation. This denitrification process results in the unavailability of NO_x to sequester the active chlorine species.

The Montreal protocol and its amendments were enacted to protect the ozone layer by phasing out the production of ozone depleting substances containing chlorine and bromine. At the most recent scientific evaluation of the effects of the treaty it was demonstrated that there is evidence of a decrease in the atmospheric burden of ozone depleting substances and that there are some signs of early stratospheric ozone recovery (WMO, 2010). Thus the monitoring of the Antarctic ozone is critical in order to evaluate the effectiveness of this treaty. In general observations provide very good constraints in our understanding about various chemical and dynamical processes on ozone.

Satellite data are used to validate Chemistry Climate Models (CCMs), which are used to predict future ozone changes (See chapter 6 from SPARC 2010 and for Antarctic ozone changes see Austin et al., 2010).

Since the discovery of the ozone hole in the 1980's the monitoring of long-term change and variability in ozone levels in the Antarctic have been intensified (WMO, 2002; WNO, 2010). Measurements provided by ground based monitoring stations are limited both in time and space. Satellite measurements can complement these existing in-situ measurements by providing a unique perspective from which to view the ozone hole, having the capability of providing daily and global long term measurements. Current ozone depletion monitoring relies on UV-vis instruments onboard satellites such as GOME (Global Ozone Monitoring Experiment), SCIAMACHY (SCanning Imaging Absorption spectroMeter for Atmospheric CartograpHY) and OMI (Ozone Monitoring Instrument), (Van Roozendael et al., 2006; Bovensmann et al., 1999; Liu et al., 2010). The lack of nighttime measurements is a severe limitation for UV-vis instruments when it comes to the monitoring of the ozone hole. As a result these instruments have large data gaps which can be filled using assimilated data (e.g. Kiesewetter et al., 2010, van der A, 2010).

Nadir-looking thermal infrared (TIR) sounders such as IASI (Infrared Atmospheric Sounding Interferometer) onboard MetOp-A complement the available datasets, with the advantage that both day and night time measurements are available at high spatial resolution. Here we present a comprehensive study of the ozone hole as viewed by IASI since the beginning of its operation and data dissemination (2008, 2009 and 2010). After a description of the instrument characteristics and the retrieval process (Sect. 2), a detailed description of the Antarctic ozone hole as observed by IASI is provided (Sect. 3). In Sects. 4 and 5 we evaluate the IASI ozone total column and profile observations along with GOME-2 (which is also onboard the MetOp-A satellite platform) data and in-situ measurements from ground based stations.

2 Ozone retrievals from IASI spectra

2.1 The IASI instrument

The IASI instrument is a high resolution, nadir viewing Fourier transform spectrometer measuring in the thermal infrared part of the spectrum, between 645 and 2760 cm^{-1}. It was launched onboard the sun synchronous polar orbiting MetOp-A satellite platform on 19 October 2006. The IASI field of view is composed of 2×2 circular pixels each with a ground footprint of 12 km at the nadir (taken every 50 km) and it has an across track scan with a swath width of 2200 km. It is characterized by a spectral resolution of 0.5 cm^{-1} (apodized) and a spectral sampling of 0.25 cm^{-1}. Depending on the surface temperature and spectral range the retrieved spectra have low radiometric noise estimated to be within the 0.1–0.4 K and around 0.2 K in the ozone 10 µm region. Due to its large spatial coverage, combined with its low radiometric noise IASI provides twice daily global measurements of key atmospheric species enabling the analysis of species concentrations, global distribution and transport such as O_3 (Boynard et al., 2009) and HNO_3 (Wespes et al., 2009). Other reactive species which are retrieved include carbon monoxide (CO) (George et al., 2009; Pommier et al., 2010), methane (CH_4) (Razavi et al., 2009), sulphur dioxide (SO_2) (Clarisse et al., 2008), ammonia (NH_3) (Clarisse et al., 2009), methanol (CH_3OH) and formic acid (HCOOH) (Coheur et al., 2009; Razavi et al., 2011). For a full detailed overview of the IASI instrument, its specifications and trace gas species that can be retrieved see Clerbaux et al. (2009).

The IASI mission delivers approximately 1.3×10^6 spectra per day, which are disseminated via Eumetcast, the EUMETSAT data distribution system, 3 h after observation. The amount of absorption contained in each spectra depends on the trace gas concentration of interest and other parameters such as surface emissivity, temperature profile, other atmospheric components which may interfere with the

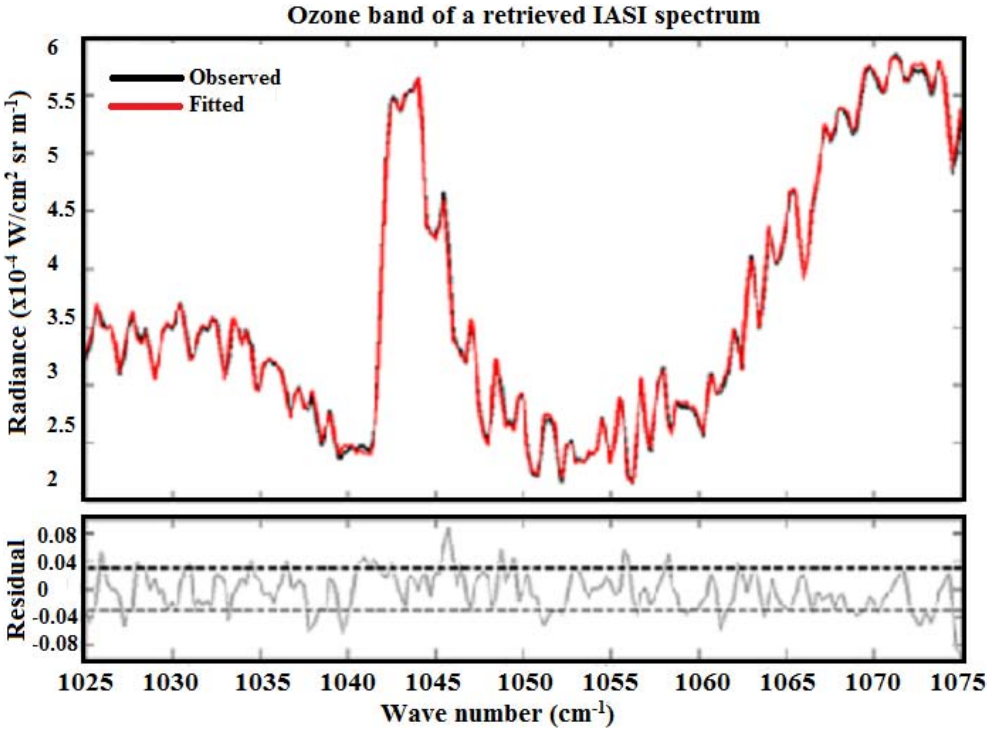

Fig. 1. Ozone absorption band region (1025 cm^{-1}–1075 cm^{-1}) of a typical IASI spectrum (observed and calculated using a radiative transfer code). The grey line in the bottom panel represents the residual of the fit which is comparable to the IASI instrument noise level (dashed line).

signal (other trace gases, clouds, aerosols, etc.) and also the characteristics of the instrument itself (spectral resolution, footprint, radiometric noise). To retrieve information about specific atmospheric trace gases from these spectra a retrieval scheme is needed.

Figure 1 shows part of the intense (high absorbing) ozone band around 9.6 µm used for retrievals. The black and red spectra represent the observed and fitted IASI spectra respectively. Both spectra clearly portray the characteristic lines in the spectrum associated with ozone absorption in the 960–1075 cm^{-1} spectral window. The grey line shows the difference between the observed and fitted spectrum. The level of instrumental noise (dashed line) is also provided for comparisons. From these spectra we retrieve both columns (total and partial) and profiles from 0 to 40 km altitude. Retrievals are performed for scenes with cloud coverage of less than 13 %, using the EUMESAT operational Level 2 (L2) cloud coverage information, temperature and humidity profiles.

2.2 IASI ozone retrievals

The challenge in developing an ozone retrieval scheme is that it should enable the fast delivery of a global, near real time product from the more than 1.3 million IASI observations per day, which are disseminated via the Eumetcast antenna system (Eumetsat, 2011). In a previous study by Boynard et al. (2009), systematic retrievals of ozone total columns were performed using an algorithm based on the Neural Network (NN) technique (Turquety et al., 2004). For the early stage IASI processing only measurements with a scan angle less than 32° on either side of the nadir were considered, and specific issues were identified over icy and sandy surfaces due to the difficulty to properly train the network with insufficient knowledge of the actual emissivity. While IASI provides a good global overview of the distributions and concentrations of ozone, the issues discussed above made it difficult to focus on particular locations such as the Antarctic. This is an area where not only were there large gaps between each overpass but also data gaps at the poles. Boynard et al. (2009) found that in general IASI ozone total columns were in good agreement with both GOME-2 and with the Brewer and Dobson ground based instruments with correlation coefficients of 0.9 and 0.85 respectively. They also found that IASI had a positive bias of about 3.3 % when compared to both GOME-2 and the ozone sondes measurements.

To allow the processing of more IASI data at any location the FORLI (Fast Optimal Retrievals on Layers for IASI) O_3 retrieval code was developed at the Université Libre de Bruxelles (ULB) to continuously retrieve ozone profiles from the IASI radiance spectra (Hurtmans et al., 2011). Figure 2 shows an ozone total column distribution above Antarctica averaged over 3 days at the peak of the 2009 ozone hole

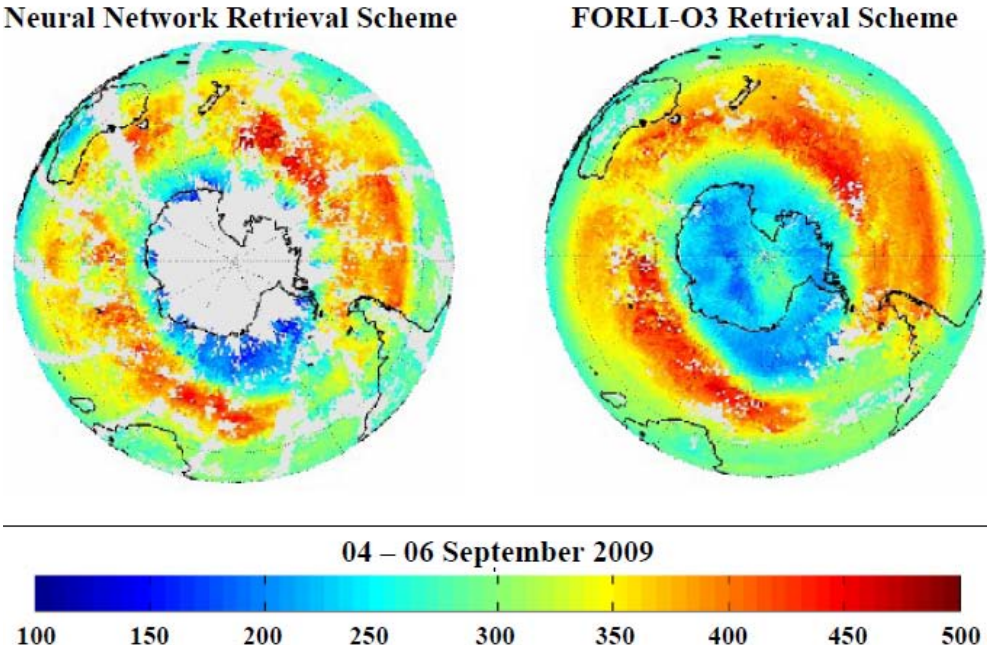

Fig. 2. IASI total ozone column distribution above Antarctica retrieved from the Neural Network scheme (left) and the FORLI-O3 scheme (right). Data are averaged over a $1^\circ \times 1^\circ$ grid and over 3 days from 4 to 6 September 2008.

(4–6 September), retrieved from the NN scheme (left panel) and from the FORLI-O3 scheme (right panel). It clearly highlights the improved capability of IASI to capture the spatial variability of total ozone columns in the Antarctic region. The FORLI scheme, unlike the initially developed NN scheme, has no limit on scan angle width, and can adjust the surface temperature, and thus processes all the data resulting in a much greater spatial coverage.

For the forward (radiative transfer) model, the code uses pre-calculated look up tables (LUTs) of absorbance at various pressures and temperatures in the spectral region of the ozone band, (960–1075 cm^{-1} spectral region, see Fig. 1). LUTs greatly minimize the computational time necessary for the retrieval of such a huge quantity of data. These tables are pre-computed on a logarithmic grid for pressure (4.5×10^{-5}–1 atm) and on a linear grid for temperature (162.8 K–322.64 K) and relative humidity for the water vapour table, using the HITRAN databases (Rothman et al., 2005, 2009). The Level 2 temperature data distributed by the Eumetcast system are used as input data for the code as well as surface emissivity from the MODIS/TERRA and IASI climatology (Wan, 2008).

The retrieval scheme is based on the Optimal Estimation Method (OEM) (Rodgers, 2000) and was developed for the retrieval of ozone profiles from high resolution nadir infrared radiances (e.g. Coheur et al., 2005). This method gives the optimal solution for a state vector $\boldsymbol{x}$ (in this case the O_3 profile), based on a given measurement y, the IASI radiance spectra, the accuracy of which is defined by an error covariance matrix $\mathbf{S}_\varepsilon$ and the equation $y = F(\boldsymbol{x}, b) + \varepsilon$, where F is the forward radiative transfer model, b represents the model parameters affecting the measurement and ε is the measurement noise.

Solving such a problem is complex as there can be many solutions that fit the observations. In order to find a meaningful solution it is necessary to constrain the results with some a priori information, by choosing the a priori profile x_a that represents the expected average profile and $\mathbf{S}_a$ the covariance matrix that ideally represents the true variability of the species about the average. The solution can be found by iteratively applying:

$$\hat{\boldsymbol{x}}_{i+1} = x_a + \mathbf{D}_y[y - F(\hat{x}_i) - \boldsymbol{K}_i(x_a - \hat{\boldsymbol{x}}_i)] \quad (1)$$

with $\mathbf{D}_y = \hat{\mathbf{S}}_i \boldsymbol{K}_i^T \mathbf{S}_\varepsilon^{-1}$ and $\hat{\mathbf{S}}_{i+1} = (\boldsymbol{K}_{i+1}^T \mathbf{S}_\varepsilon^{-1} \boldsymbol{K}_{i+1} + \mathbf{S}_a^{-1})^{-1}$ where $\boldsymbol{K}_i = \left(\frac{\partial F}{\partial x}\right)_i$ is the Jacobian at state $\boldsymbol{x}_i$, $\boldsymbol{K}_i^T$ is its transpose and $\hat{\boldsymbol{x}}_{t+1}$ is the new state vector. The matrix $\mathbf{D}_y$ is the matrix of contribution factors or gain matrix and the error covariance of the solution is given by $\mathbf{S}_{t+1}$. The iteration starts with some initial estimate of the state, the a priori information x_a, and the covariance matrix $\mathbf{S}_a$, and terminates when convergence is reached.

The choice of a priori information is an important step for the construction of the retrievals in the infrared. The FORLI-O3 a priori profile and associated covariance matrix were constructed using the Logan/Labow/McPeters climatological database (McPeters et al., 2007). This ozone climatology is altitude dependent and consists of monthly averaged ozone profiles for 10° latitude zones from 0 to 60 km. This climatology is a combination of data from the Stratospheric

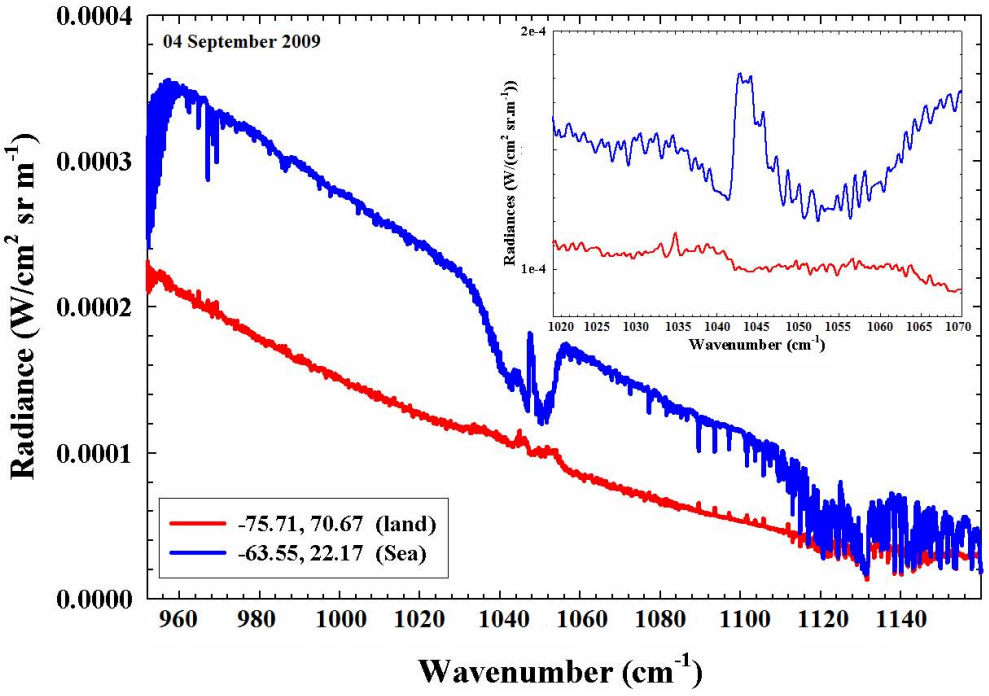

Fig. 3. Illustration of two IASI radiance spectra, taken over the Antarctic. The blue spectrum is representative of spectra over the ocean close to the Antarctic and the red spectrum over the Antarctic continent itself. Inset into the figure are the same spectra but shown for a narrower spectral range where ozone absorbs. See Fig. 4 for the location of both measurements.

Aerosol and Gas Experiment II (SAGE II; 1988–2001), the Microwave Limb Sounder (MLS; 1991–1999) and data from ozone sondes (1988–2002). Such a global climatology aids in the construction of a priori information as it represents a good approximation of the average state of the atmosphere.

To allow for a useful comparison with other data sets, a smoothing of the true retrieval state is necessary and is characterized as follows by Eq. (2).

$$\hat{x} = \mathbf{A}x + (I - \mathbf{A})x_\alpha \quad (2)$$

where $\hat{x}$ is the retrieved profile, $\mathbf{A}$ is the averaging kernel matrix, x is the true profile and x_a is the a priori profile. The averaging kernels indicate the measure of sensitivity of the retrieved state $\hat{x}$ to the true state x. The trace of $\mathbf{A}$, representing the degrees of freedom for the signal (DOFs), measures the number of independent pieces of information available from the retrieval and gives an estimation of the vertical sensitivity of the retrievals. FORLI-O3 generates ozone partial columns in 40, 1 km thick layers, along with the associated averaging kernels and errors matrices.

3 The Antarctic ozone hole as seen by IASI

Figure 3 shows two IASI infrared spectra taken over the Antarctic in September 2009 and the ozone absorption band for each spectrum is highlighted in the inset. The blue spectrum is representative of spectra over the ocean close to main land Antarctica and the red spectrum is representative of those taken over the Antarctic continent itself (both measurements are located in map plots provided in Fig. 4, marked B and A respectively).

Over the ocean the spectrum shows significant strength in the ozone absorption band in the thermal infrared. However, over the ice caps, although the ozone band is observed, it is weaker and the absorption lines seem to disappear as part of the vertical information is lost because of the low ozone content.

A global distribution of the DOFs and the averaging kernels associated with each of these spectra are depicted in Fig. 4. This figure highlights the difficulties in retrieving ozone concentrations over the Antarctic region. As previously discussed, the DOFs are a measure of the vertical sensitivity of the measurement, i.e. the higher the number of DOFs the more vertical layers can be discriminate. Figure 4 (left) shows that over the ocean, the DOFs generally range between 3 and 4, while over the ice caps the DOFs range between 1 and 2. Because of the weaker signal over the ice, part of the vertical information is lost. These results indicate that care is needed when selecting spectra over the Antarctic land mass. As shown in Fig. 4, the averaging kernels associated with the measurement over the ocean are better defined (DOFs of 3.3) than those associated with the measurement taken over the ice (DOFs of less than 1.5).

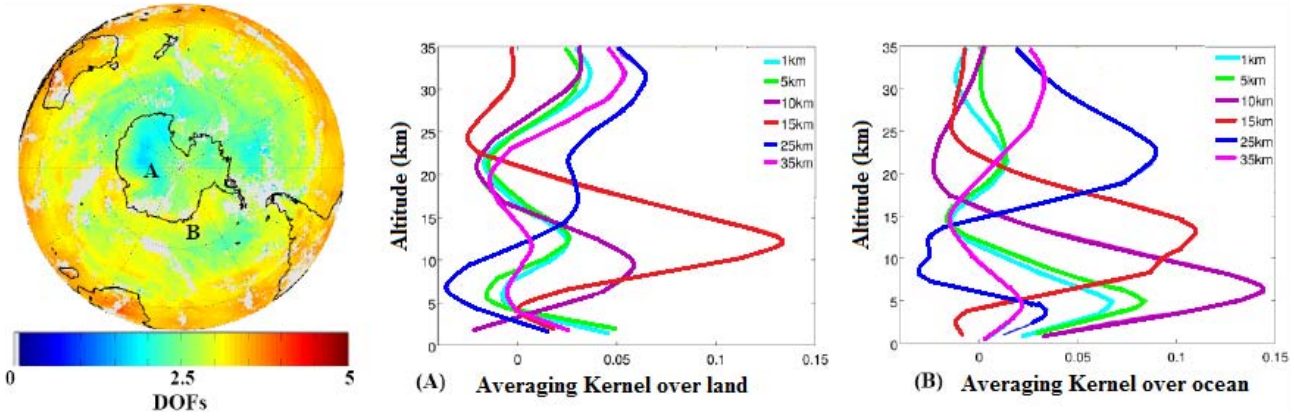

Fig. 4. IASI DOFs distribution above Antarctica (grey is for no data), along with averaging kernel functions for partial columns of different altitudes characterizing the retrievals from spectra shown in Fig. 3, over land **(A)** and over ocean **(B)**, respectively.

The ozone hole area is defined as the region located south of 40° S where ozone values fall below the threshold value of 220 DU (WMO, 2002). Recent studies have shown that during the 1980s the ozone hole over Antarctica expanded rapidly, this expansion slowed in the 1990s. In the last few years this expansion and ozone loss rates have appeared to level off (Newman et al., 2009; Austin et al., 2010).

Figure 5 shows an example of ozone maps over the Antarctic during the ozone hole period. The maps plot the weekly averaged IASI ozone total columns on a $1° \times 1°$ grid for September of 2008, 2009 and 2010. This period marks the time when the ozone hole area approaches maximum. Such distribution maps show that the size, shape and evolution of the ozone hole can be clearly monitored.

Figure 6 depicts the daily evolution of IASI total ozone (black lines), retrieved from FORLI-O3 and averaged over 5° latitude bands from 50° S to 90° S, from the beginning of August 2008 to the end of December 2010. It is worth noting here that FORLI-O3 algorithm has been upgraded several times since its development and as such this data set was obtained using slightly different versions of the algorithm. The changes between the different versions are minor and should not impact this study. The shaded grey area represents the standard deviation ($\pm\sigma$) about this average. Apart from a few spurious points, the spread of the data is minimal for all periods outside the ozone hole period. The highlighted blue area represents the ozone hole period, August to December of each year. This figure clearly illustrates the seasonal cycle of ozone reduction over the Antarctic during polar spring (WMO, 2010). For all years distinct features exist. One such feature is that the ozone hole itself forms annually south of 60° S. Another is that north of 60° S there is a noticeable rise in ozone concentrations during the ozone hole periods which are representative of the edge of the vortex surrounding the ozone hole. Moving southwards it is also evident that the decrease in ozone concentrations and the longevity of the hole itself become more pronounced. Each year the peak of the ozone hole occurs by mid September and at this time ozone concentrations are seen to decrease by more than 50 % south of 75° S to approximately 150 DU.

Despite these well observed trends there are some inter-annual variations. In 2009 there was a sharp increase in ozone concentrations in mid October (circled areas) that is not visible in 2008 or 2010. Figure 7 illustrates that during this period the ozone hole became more elliptical in shape and off-centre relative to the South Pole. This is usually caused by enhanced planetary wave activity leading to a perturbation of the polar vortex and an increase in ozone transport (e.g. Weber et al., 2003; von Savingny et al., 2005). By 22 October the polar vortex had reverted back to the more standard circular rotation and ozone concentrations returned to levels similar to those before the perturbation. In 2010 there was a relatively slow start to the ozone hole formation (the beginning of September as opposed to mid August) in comparison with other years (see Fig. 6). This was mainly due to higher than average temperatures in the stratosphere over the Antarctic resulting in the reduction in the volume of polar stratospheric clouds in mid to late August of this year. Also in 2010 the ozone hole period extended into late December with ozone values not rising above the 220 DU threshold until 21 December. For this 3 yr study the ozone hole area was at its largest for this time of the year.

Figure 8 (solid lines) illustrates the evolution of the ozone hole area from August to the end of December for 2008 (green), 2009 (blue) and 2010 (red). It is compiled from weekly averaged area values of the ozone hole from $1° \times 1°$ grid resolution data sets. Of the three years studied, 2008 (green) proved to be the year with the largest ozone hole area and persisted well into December. The maximum hole area occurred at the end of September and reached values of more than 25 million square kilometers. In 2009 the ozone hole (blue) had a shorter lifetime than 2008 and was less severe, beginning again in mid August and dissipating by the end of November. In September the ozone hole area

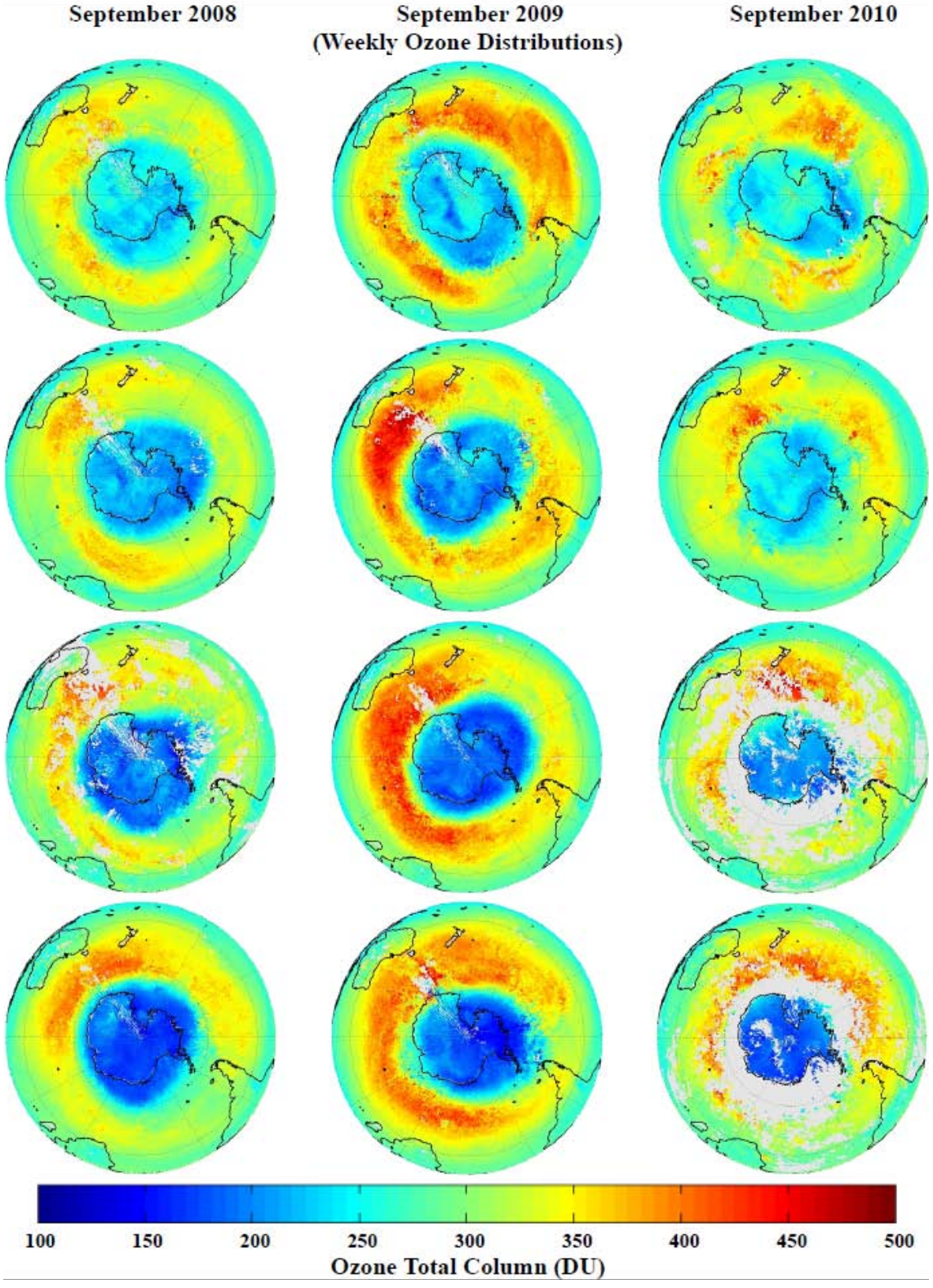

Fig. 5. IASI total ozone distribution above Antarctica (DU) retrieved using the FORLI-O3 algorithm. Data are averaged over a 1°x1° grid and over each week in the peak month (September) during the ozone hole period for 2008, 2009 and 2010. For the two last weeks of September 2010 the data are more sparse because part of the L2 temperature data was not provided by EUMETSAT.

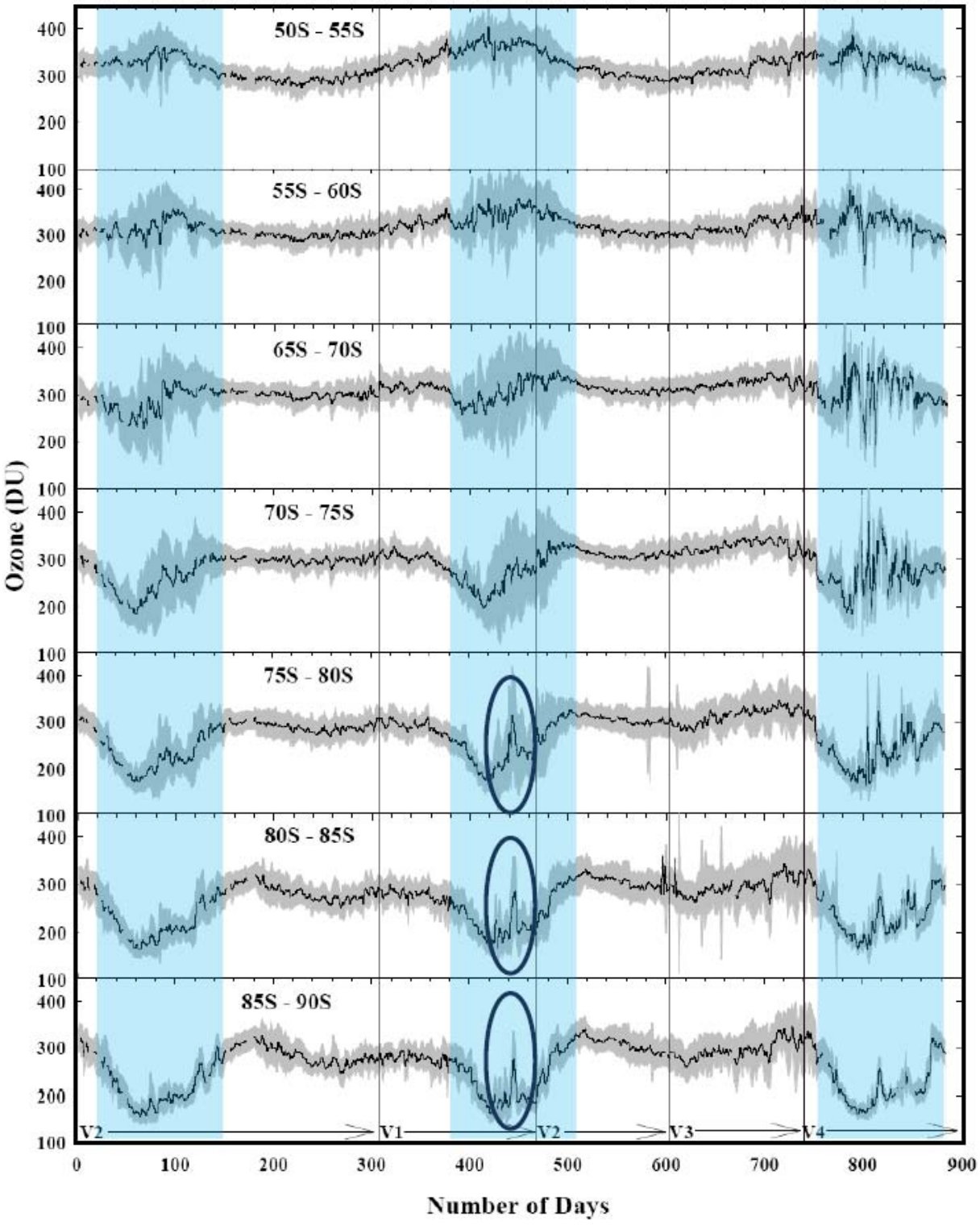

Fig. 6. Daily time series from August 2008 to December 2010 showing the evolution of the total for each day at 5 degree latitude increments from 50° S to 90° S. The daily measurements are described by the black line, the shaded grey represents the standard deviation about the average and the shaded blue area represents the ozone hole period. Version 1, 2, 3 and 4 (V1, V2, V3 and V4 respectively) are different versions of the FORLI-O3 program, numbered according to the date they were implemented (vertical lines). The circled areas highlight some inter-annual variability which is discussed in the text.

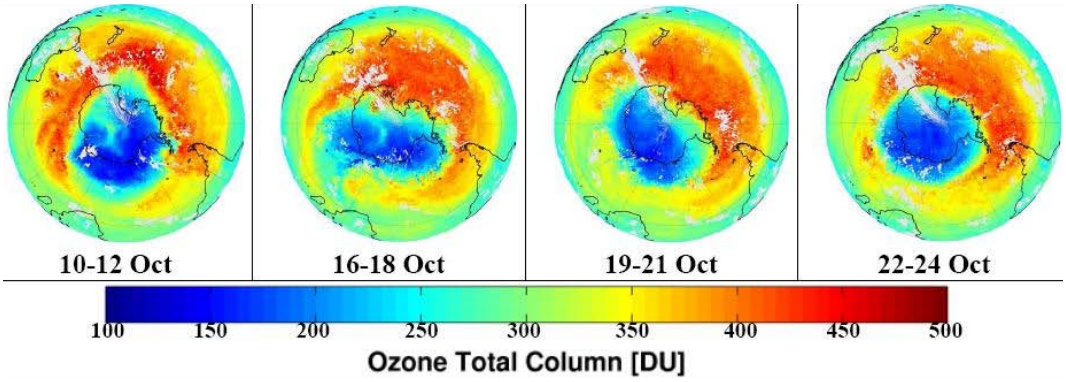

Fig. 7. Total ozone column distributions above Antarctica averaged over 3 day periods in October 2009. The change from a circular to elliptical rotation and back again is clearly visible. Data are averaged over a $1° \times 1°$ grid.

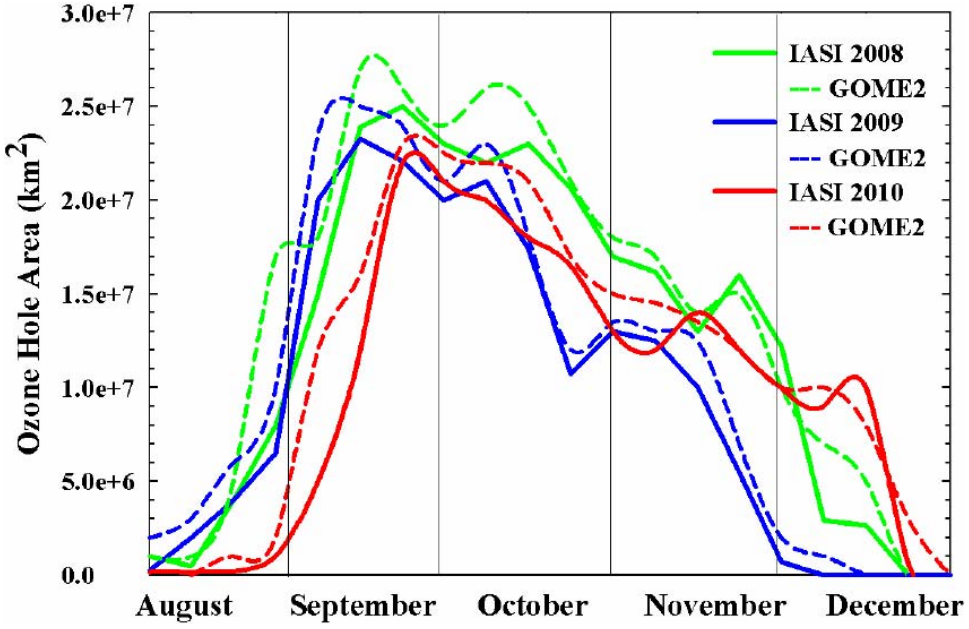

Fig. 8. Evolution of the ozone hole area (defined as the area with less than 220 DU) as measured from IASI (solid line) and GOME-2 (dashed line) for 2008 (green), 2009 (blue) and 2010 (red). This data set is compiled from weekly averaged data from $1° \times 1°$ degree resolution datasets.

was at its greatest with an area size of approximately 24 million square kilometers. For 2010 (red) the ozone hole area expansion began in the beginning of September, much later than previous years and its maximum area reached 21 million square kilometers. However despite 2010 being less severe, its area declined less rapidly than in the previous years with the ozone hole period extending well into late December before dissipating off.

4 Comparison with GOME-2 ozone total columns

As previously discussed, the UV-vis instrument GOME-2 is also on board the MetOp-A platform. In this section we compare IASI and GOME-2 ozone total column retrievals during the Antarctic ozone hole. GOME-2 is a UV-vis, cross track, nadir viewing spectrometer working in the 240–790 nm spectral range. It has a default field of view of $80 \times 40\,\mathrm{km}^2$ and it has a swath width of approximately 1920 km providing almost daily coverage at the equator. The GOME-2 total ozone column is calculated as a vertically integrated ozone profile based on the vertical ozone profile retrieval algoritm OPERA developed and run operationally in near real time by KNMI in the framework of the EUMETSAT O3MSAF.

For this study both IASI and GOME-2 total column ozone distributions were averaged to a $1° \times 1°$ grid. As the GOME-2 measurements are not available during polar night,

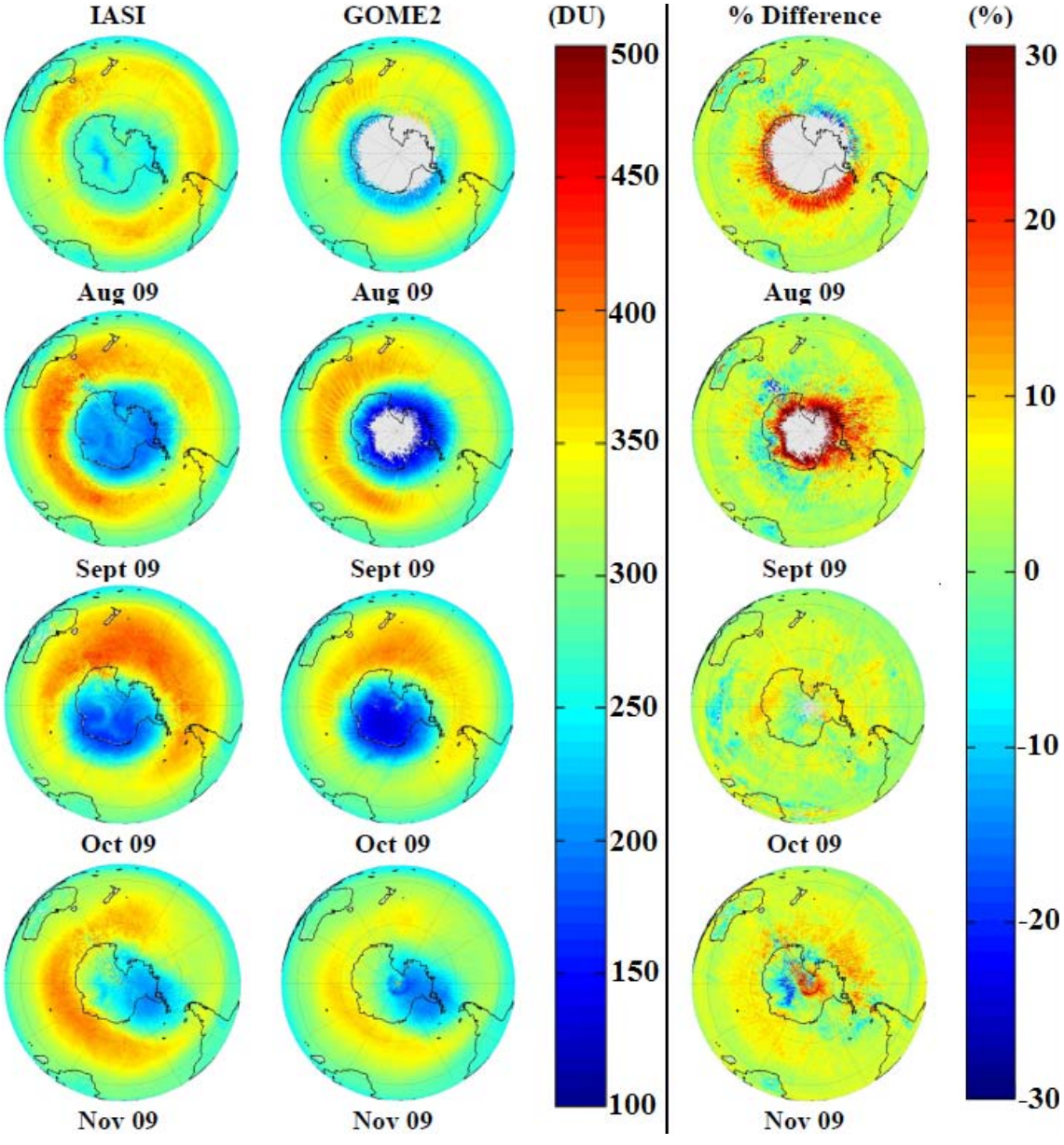

Fig. 9. IASI and GOME2 total ozone monthly mean distribution for the ozone hole period of 2009 along with the percentage difference between both instruments.

IASI observations during this period without sunlight were excluded from the following analysis.

The ozone hole area as observed from GOME-2 for 2008–2010 is presented in Fig. 8. It is clear that in general IASI and GOME-2 compare quite well, observing similar peaks and similar beginning and end periods during these 3 yr. GOME-2 however did measure a marginally larger ozone hole for all 3 yr with the maximum difference of 7.5 % measured between the two instruments in 2008.

Figure 9 shows the monthly mean distributions of total ozone for both IASI and GOME-2 (first and second columns respectively) over the Antarctic region for the ozone hole season, August to November 2009. Despite the effect of GOME-2 being unable to measure during polar night, both instruments show similar results. As expected for each month maximum total ozone is observed at the edge of the polar vortex and minimum total ozone is observed within the ozone hole. The temporal and spatial evolution of the ozone hole throughout the period is also well observed by both instruments.

The third column in Fig. 9 presents the percentage difference between IASI and GOME-2. Despite both instruments observing similar features for all months, IASI in general measures between 5 %–10 % higher ozone than

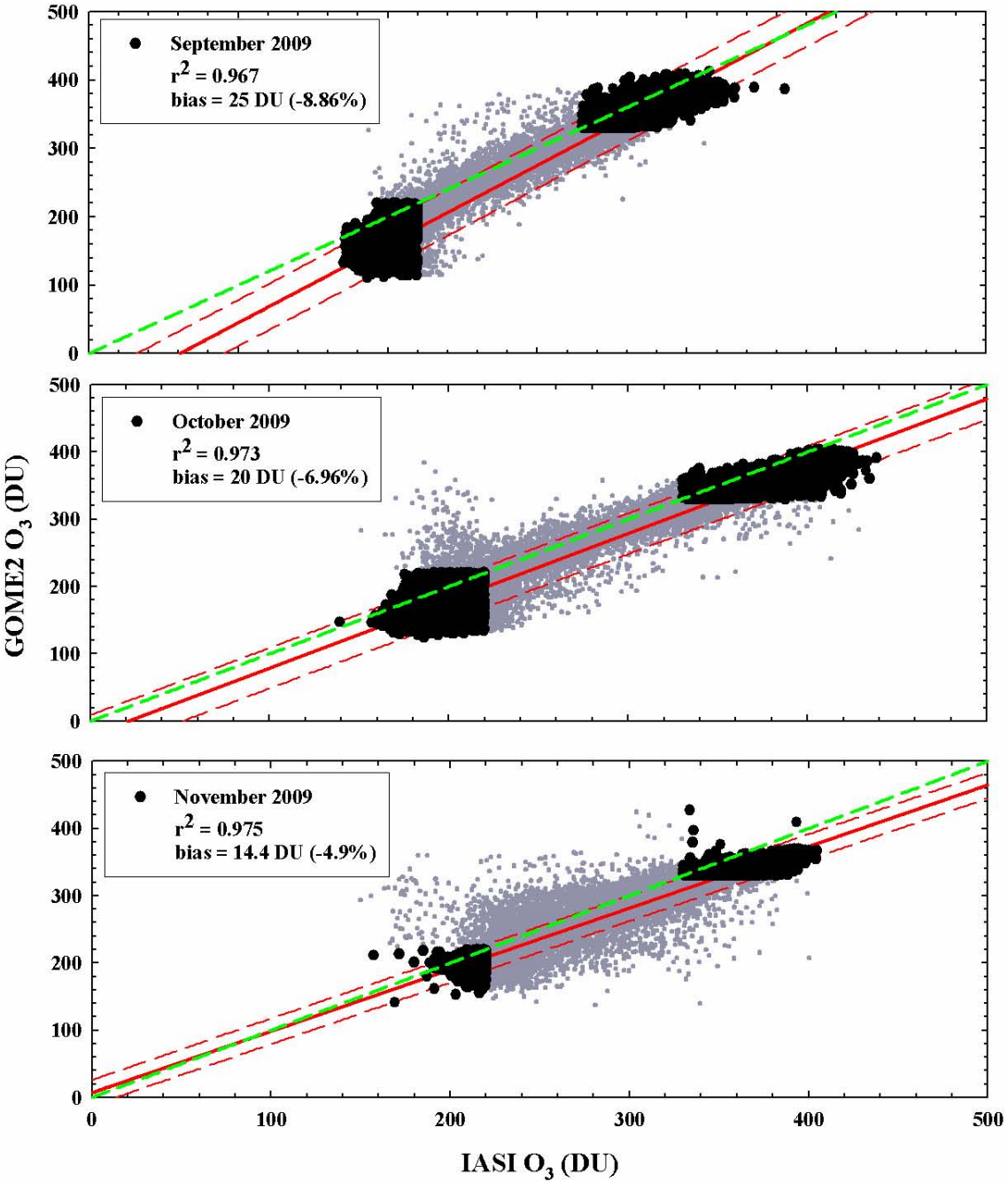

Fig. 10. Ozone correlation between GOME-2 and IASI for September (top panel), October (middle panel) and November (bottom panel) of 2009. The black data below 220 DU and above 320 DU represent the low ozone values within the ozone hole and the higher values associated with the edge of the vortex respectively. The grey data represents all other data south of 45° S, the area for which the ozone hole is defined, which do not lie within the hole or vortex regions. The linear regressions (solid red line), confidence intervals (dashed red lines) and 1:1 ratios (dashed green line) are also represented. The average bias is also presented.

GOME-2. The predominant difference occurs during the August and September periods where IASI has a positive bias of between 20 %–30 % surrounding the ozone hole core, where for these periods GOME-2 measures a larger decrease than IASI within the ozone hole itself. In November there is a negative bias within the hole area as IASI measures a slightly larger elongated ozone hole than GOME-2. Inside the hole for all months a positive bias of approximately 7–8 % is also observed as IASI measures larger concentrations than GOME-2. However in general the difference between

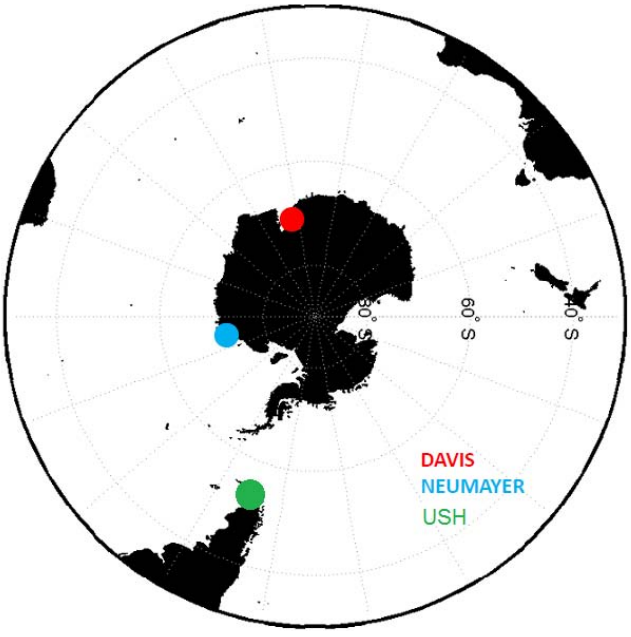

Fig. 11. Geographic locations of the three ground based stations used for the IASI/ozone sonde profile comparison; Davis in red, Neumayer in blue and USH in green.

the two instruments remains below 10 %. Previous studies (e.g. Schneider et al., 2008; Anton et al., 2011) have shown a similar bias (of approximately 5 %) between TIR and UV-vis observations and this may be due to discrepancies of spectroscopic parameters betweeb the UV and TIR spectral regions. A recent study by Massart et al. (2009), also found that IASI tends to overestimate the ozone total columns by 2–8 %, in comparison to a model forced by the total columns retrieved from MLS (MicroWave Limb Sounder) and SCIAMACHY (Scanning Imaging Absorption spectrometer for Atmospheric Cartography).

Figure 10 presents a statistical comparison between IASI and GOME-2 ozone total columns that was performed for September, October and November of 2009. The correlation coefficients and the bias about the mean are inset into the graph for each month. The black data below 220 DU and above 320 DU represent ozone values inside and at the edge of the ozone hole respectively. The grey data represents all other data south of 45° S. The linear regression for each month (solid red lines), the confidence intervals (dashed red lines) and the 1:1 ratio reference line (dashed green line) are also presented in the figure. It is clear from the strong correlation coefficients for each month ($r^2 = 0.967$, $r^2 = 0.973$ and $r^2 = 0.975$) that IASI and GOME-2 are closely comparable throughout the entire ozone hole region and period. Based on these regression lines IASI shows a slight positive bias as discussed before.

Both instruments compare quite well, though slight differences in the measurement of the ozone hole area and shape by IASI and GOME-2 give rise to some spurious data points in this region. This is particularly the case in October and November where GOME-2 measures some higher ozone concentrations than IASI in the ozone hole. Though as already discussed above there is an identified bias between the two instruments and efforts should be made to fully understand this, some differences between the instruments can be attributed to the different modes of observation which have not been accounted for in this analysis. For example both instruments have a different ground footprint and observation geometry and thus are subject to different cloud contamination and probe different air masses. Both instruments also have different vertical sensitivities, IASI has a maximum sensitivity to the ozone profile in the upper troposphere – lower stratosphere while GOME-2 has a maximum sensitivity in the stratosphere. It is worth noting that IASI relies on the a priori climatology when low levels of ozone occur, eg inside the ozone hole.

5 Comparison with ozone sondes

The in-situ ozone-sonde profile measurements used in this study are from the World Ozone and Ultra Violet Radiation Data Centre (WOUDC) data base and the location indicated in Fig. 11 are the German Neumayer station (78°39′ S; 08°15′ W, WMO no. 323), the Australian Davis station (68°35′ S; 77°58′ E, WMO no. 450) and the Argentinian USH station (54°88′ S; 68°19′ W, WMO no. 339) in blue, red and green respectively. Each station is equipped with electrochemical concentration cell (ECC) ozone-sondes which utilize the oxidation reaction of ozone with potassium iodide to determine the ozone profile. These ozone-sondes measure up to 30 km altitude.

It should be noted that over this particular region finding a triple collocation between IASI, GOME-2 and an ozone sonde was not possible because ozone sonde measurements are not daily and GOME-2 due to its geometry may be scanning a different location from IASI and the ozone sonde. The primary challenge of comparing IASI and ozone sonde measurements is the relatively small number of co-incident measurements between satellite and sondes in the Antarctic. A set of strict co-incidence criteria were applied. Only those measurements that were co-located in space to within 0.5° and co-located in time to within 6 h were chosen. For the cases where two or more such IASI profiles met the criteria, a mean profile was calculated for the comparison.

Secondly, the difference in vertical resolution and sensitivity between the two data sets were accounted for. The IASI averaging kernel and a priori constraints were applied to the ozone-sonde data following Eq. (2), producing a vertical profile that represents what IASI would measure for the same air sampled by the sonde. For a more in-depth description of this method see Rodgers (2000).

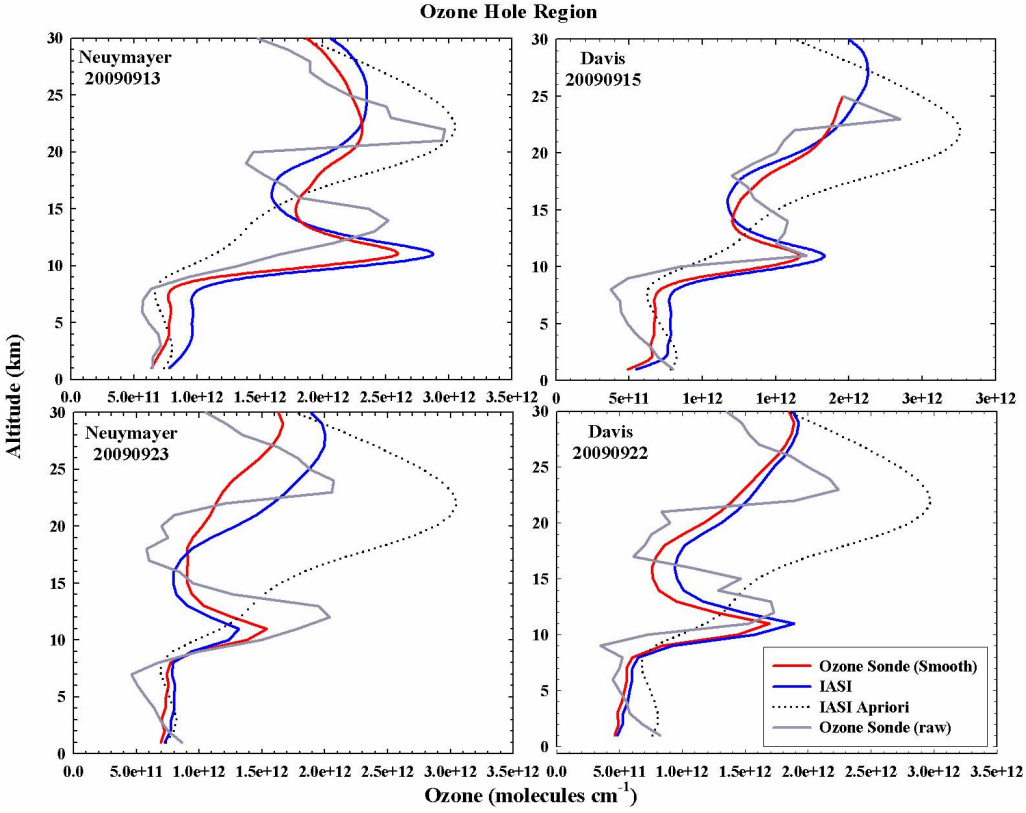

Fig. 12. Comparisons between IASI and ozone sonde profiles measured within the ozone hole at the Neumayer (left) and Davis (right) stations for different days of September 2009. The IASI a priori is represented by the black dotted line. The IASI profile is an averaged profile of between 5 and 10 profiles (depending on the location), co-located in time and space to the ozone sonde measurements (raw data interpolated at the IASI altitude). The ozone sonde profile (in grey) has been convolved with the IASI averaging kernels (in red). Note that the a priori profile here has been converted from mixing ratios (independent of temperature and pressure) to density (dependent on temperature and pressure). Thus if temperature and pressure change from one location or day to another, different a priori profiles in density will be found.

Finally it should be noted that the sonde data are supplied in units of ozone partial pressure on a vertical scale of atmospheric pressure while the IASI data are supplied in molecules cm^{-3} on a vertical scale of atmospheric height. Therefore before the ozone-sonde data can be convolved with the IASI averaging kernels, the vertical scales and the units must be homogenized via a simple extrapolation and unit conversion as follows:

$$n = 10^{-9} \frac{F_{\text{part}}}{k\tau} \tag{3}$$

where n is in molecules cm^{-1}, P_{part} is the ozone partial pressure in hPa, k is the Boltzmann constant (1.3807×10^{-23} J K^{-1} molecule^{-1}) and T (retrieved) is the temperature in K.

Figure 12 shows an example of an IASI and ozone-sonde profiles (blue and red profiles respectively) taken from within the ozone hole during September 2009. The IASI a priori profile (dotted black profile) is also represented for each location. As previously discussed in Sect. 2.2 retrieving ozone profiles with IASI over the ice can prove difficult thus it should be noted that the averaging kernels for each collocation between IASI and the ozone-sonde were closely studied and only those measurements with well defined averaging kernels (i.e. that are equally distributed vertically for better vertical coverage) and DOFs greater than or equal to 3 were chosen for this comparison.

The same features are observed by both instruments such as the notable decrease in ozone concentrations between 15–20 km, however IASI slightly overestimates in the lower troposphere for all cases.

Inside the ozone hole (Fig. 13) for the USH and Davis stations IASI compares well to the convolved ozone sondes with only marginal differences in shape and magnitude. In the troposphere there is almost no difference while in the stratosphere IASI slightly overestimates in comparison to the USH station and underestimates for the Davis station. IASI and the sondes compare to within 20 % and within 30 % for the other two cases. This demonstrates just how accurately IASI can estimate the shape and size of ozone profiles during the ozone hole period.

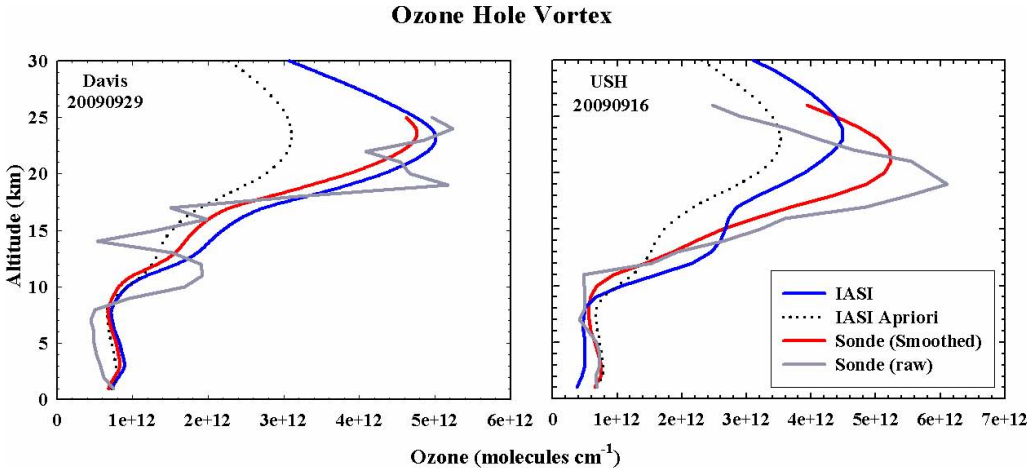

Fig. 13. Comparison between IASI and ozone sonde profiles measured in the Antarctic vortex at the Davis and USH stations for different days in September 2009. The IASI a priori is represented by the black dotted line. The IASI profile is an averaged profile of a number of profiles co-located in time and space to the ozone sonde measurements. The ozone sonde profile (in grey) has been convolved with the IASI averaging kernels (in red).

6 Summary and conclusion

This paper presents an assessment of the capabilities of IASI to perform continuous, precise measurements of the ozone hole. IASI will fly continuously for the next 10 yr (on MetOp-B and -C). As already reported for CO in Pommier et al. (2010), polar regions are at the same time easy to observe as they are well covered by the MetOp polar orbiting satellite, but on the other hand difficult to process due to the specific low temperature and thermal contrast conditions and frozen surfaces that impact the radiance spectra. In this work, the FORLI-O3 retrieval scheme was utilized. This retrieval algorithm allows the processing of global distributions of ozone two times per day, in near real time, from all the IASI spectra with cloud contamination of less than 13 %.

In this work we analyze the IASI ozone total columns distributions over the Antarctic to study the ozone hole evolution in 2008, 2009 and 2010. Our results highlight the capability of IASI to capture very precisely the short term spatial and temporal variability of the ozone hole development, also during polar night. Data comparisons between IASI and GOME-2 observations of the ozone total column were performed for the three ozone hole periods and showed excellent agreement for both the timing and area of the ozone hole. A detailed comparison for 2009 provided correlation coefficients of 0.97 for September, October and November. IASI showed an average positive bias of approximately 7 %. This is in line with previous research by Boynard et al. (2009) who found an average positive bias of between 3 %–5 % on a global scale.

The retrieval of ozone vertical profiles from IASI spectra collocated with ozone sonde measurements for September 2009 was also performed. Here we found that IASI showed good agreement with the sonde measurements from the troposphere to the stratosphere, with the difference between IASI and the sondes being less than 30 % inside the ozone hole. IASI was also found to be very sensitive to the ozone profile in the lower stratosphere between 15–20 km, remarkably capturing the vertical extent of the ozone hole, as shown by the good agreement with the ozone sondes.

Such continuous IASI ozone measurements are complementing existing data in the long term trend assessment of ozone which suggests that the ozone hole expansion and ozone loss rates have appeared to have stopped (WMO, 2010).

Work is in progress to combine the IASI and GOME-2 profile products to derive improved profiles. Theoretical studies have shown that improvements in measuring the troposphere could be achieved via the combination of complimentary UV and TIR measurements (Zhang et al., 2010; Worden et al., 2007).

Acknowledgements. IASI has been developed and built under the responsibility of the Centre National des Etudes Spatiales (CNES, France). It is flown onboard the MetOp satellites as part of the EUMETSAT Polar System. The IASI level 1 data are distributed in near real time by EUMETSAT through the Eumetcast dissemination system. The authors acknowledge the Ether French atmospheric database (http://ether.ipsl.jussieu.fr) for providing the IASI data. The GOME-2 level 2 data were provided by the DLR and KNMI through Eumetcast. These data were generated under the auspices of the O3M SAF project of EUMETSAT. The ozone sonde data used in this work were provided by the World Ozone and Ultraviolet Data Centre (WOUDC), the Southern Hemisphere Additional Ozone sondes (SHADOZ) and the Global Monitoring Division (GMD) of NOAA's Earth System Research Laboratory and are publically available (http://www.woudc.org, http://croc.gsfc.nasa.gov/shadoz

and http://www.esrl.noaa.gov/gmd). All the agencies cited above are acknowledged for providing data. The research in France was conducted with the financial support of CNES. The research in Belgium was funded by the "Actions de Recherche Concertées" (Communauté Française), the Fonds National de la Recherche Scientifique (FRS-FNRS F.4511.08), the Belgian State Federal Office for Scientifique, Technical and Cultural Affairs and the European Space Agency (EAS-Prodex C90-327).

Edited by: M. Weber

The publication of this article is financed by CNRS-INSU.

References

Antón, M., D. Loyola, C. Clerbaux, M. López, J. M. Vilaplana, M. Bañón, J. Hadji-Lazaro, P. Valks, N. Hao, W. Zimmer, P. F. Coheur, D. Hurtmans, and L. Alados-Arboledas: Validation of the Metop-A total ozone data from GOME-2 and IASI using reference ground-based measurements at the Iberian Peninsula, Remote Sens. Environ., 115, 1380–1386, 2011.

Austin, J., Struthers, H., Scinocca, J., Plummer, D. A., Akiyoshi, H., Baumgaertner, A. J. G., Bekki, S., Bodeker, G. E., Braesicke, P., Brühl, C., Butchart, N., Chipperfield, M. P., Cugnet, D., Dameris, M., Dhomse, S., Frith, S., Garny, H., Gettelman, A., Hardiman, S. C., Jöckel, P., Kinnison, D., Kubin, A., Lamarque, J. F., Langematz, U., Mancini, E., Marchand, M., Michou, M., Morgenstern, O., Nakamura, T., Nielsen, J. E., Pitari, G., Pyle, J., Rozanov, E., Shepherd, T. G., Shibata, K., Smale, D., Teyssèdre, H., and Yamashita, Y.: Chemistry-climate model simulations of spring Antarctic ozone, J. Geophys. Res., 115, D00M11, doi:10.1029/2009JD013577, 2010.

Balis, D. S. and Bojkov, R. D. : Characteristics of Antarctic Spring ozone decline from satellite and ground based measurements from the appearance of the "ozone hole" up to December 2001. Proc. Of the 6th Europ. Symp. On Stratospheric Ozone in Goeteborg, Sweden, edited by: Harris, N., Amanatidis, G., and Levine, J., Europ. Com. Air Pollution Research Report No. 79, 39–42, 2003

Bovensmann, H., Burrows, J. P., Buchwitz, M., Frerick, J., Noël, S., Rozanov, V. V., Chance, K. V., and Goede, A. P. H., SCIAMACHY - Mission objectives and measurement modes, J. Atmos. Sci., 56, 127–150, 1999.

Boynard, A., Clerbaux, C., Coheur, P.-F., Hurtmans, D., Turquety, S., George, M., Hadji-Lazaro, J., Keim, C., and Meyer-Arnek, J.: Measurements of total and tropospheric ozone from IASI: comparison with correlative satellite, ground-based and ozonesonde observations, Atmos. Chem. Phys., 9, 6255–6271, doi:10.5194/acp-9-6255-2009, 2009.

Clarisse, L., Coheur, P. F., Prata, A. J., Hurtmans, D., Razavi, A., Phulpin, T., Hadji-Lazaro, J., and Clerbaux, C.: Tracking and quantifying volcanic SO2 with IASI, the September 2007 eruption at Jebel at Tair, Atmos. Chem. Phys., 8, 7723–7734, doi:10.5194/acp-8-7723-2008, 2008.

Clarisse, L., Clerbaux, C., Dentener, F., Hurtmans, D., and Coheur, P.-F.: Global ammonia distribution derived from infrared satellite observations, Nat. Geosci., 2, 479–483, doi:10.1038/ngeo551, 2009

Clerbaux, C., Boynard, A., Clarisse, L., George, M., Hadji-Lazaro, J., Herbin, H., Hurtmans, D., Pommier, M., Razavi, A., Turquety, S., Wespes, C., and Coheur, P.-F.: Monitoring of atmospheric composition using the thermal infrared IASI/MetOp sounder, Atmos. Chem. Phys., 9, 6041–6054, doi:10.5194/acp-9-6041-2009, 2009.

Coheur, P.-F., Barret, B., Turquety, S., Hurtmans, D., Hadji-Lazaro, J., and Clerbaux, C. : Retrieval and characterization of ozone vertical profiles from a thermal infrared nadir sounder, J. Geophys. Res., 110, D24303, doi:10.1029/2005JD005845, 2005.

Coheur, P.-F., Clarisse, L., Turquety, S., Hurtmans, D., and Clerbaux, C.: IASI measurements of reactive trace species in biomass burning plumes, Atmos. Chem. Phys., 9, 5655–5667, doi:10.5194/acp-9-5655-2009, 2009.

De Laat, A. T. J., R. van der A, J., Allaart, M. A. F., van Weele, M., Benitez, G. C., Casiccia, C., Paes Leme, N. M., Quel, E., and Salvador, J., Wolfram, E.: Extreme sunbathing: Three weeks of small total O_3 columns and high UV radiation over the southern tip of South America during the 2009 Antarctic O_3 hole season, Geophys. Res. Lett., 37, L14805, doi:10.1029/2010GL043699, 2010

Eumetsat TD 18 Metop-A Direct Readout AHRPT Technical Description, EUM/OPS/TEN/08/1663, v1J, available at: www.eumetsat.int, last access: 28 March 2011, 2011.

Feng, W., Chipperfield, M. P., Davies, S., Sen, B., Toon, G., Blavier, J. F., Webster, C. R., Volk, C. M., Ulanovsky, A., Ravegnani, F., von der Gathen, P., Jost, H., Richard, E. C., and Claude, H.: Three-dimensional model study of the Arctic ozone loss in 2002/2003 and comparison with 1999/2000 and 2003/2004, Atmos. Chem. Phys., 5, 139–152, doi:10.5194/acp-5-139-2005, 2005.

Feng, W., Chipperfield, M. P., Davies, S., Mann, G. W., Carslaw, K. S., Dhomse, S., Harvey, L., Randall, C., and Santee, M. L.: Modelling the effect of denitrification on polar ozone depletion for Arctic winter 2004/2005, Atmos. Chem. Phys., 11, 6559–6573, doi:10.5194/acp-11-6559-2011, 2011.

Fortuin, J. P. F. and Kelder, H.: An ozone climatology based on ozone sonde and satellite measurements, J. Geophys. Res., 103, 31709–31734, 1998

George, M., Clerbaux, C., Hurtmans, D., Turquety, S., Coheur, P.-F., Pommier, M., Hadji-Lazaro, J., Edwards, D. P., Worden, H., Luo, M., Rinsland, C., and McMillan, W.: Carbon monoxide distributions from the IASI/METOP mission: evaluation with other space-borne remote sensors, Atmos. Chem. Phys., 9, 8317–8330, doi:10.5194/acp-9-8317-2009, 2009.

Hurtmans, D., Coheur, P.-F., Wespes, C., Clarisse, L., Scharf, O., Clerbaux, C., Hadji-Lazaro, J., George, M., and Turquety, S.: FORLI radiative transfer and retrieval code for IASI, JQSRT, under review, 2011.

Kiesewetter, G., Sinnhuber, B.-M., Vountas, M., Weber, M., and Burrows, J. P.: A long-term stratospheric ozone data set from assimilation of satellite observations: High-

latitude ozone anomalies, J. Geophys. Res., 115, D10307, doi:10.1029/2009JD013362, 2010.

Liu, X., Bhartia, P. K., Chance, K., Froidevaux, L., Spurr, R. J. D., and Kurosu, T. P.: Validation of Ozone Monitoring Instrument (OMI) ozone profiles and stratospheric ozone columns with Microwave Limb Sounder (MLS) measurements, Atmos. Chem. Phys., 10, 2539–2549, doi:10.5194/acp-10-2539-2010, 2010.

Massart, S., Clerbaux, C., Cariolle, D., Piacentini, A., Turquety, S., and Hadji-Lazaro, J.: First steps towards the assimilation of IASI ozone data into the MOCAGE-PALM system, Atmos. Chem. Phys., 9, 5073–5091, doi:10.5194/acp-9-5073-2009, 2009.

Maturilli, M., Neuber, R., Massoli, P., Cairo, F., Adriani, A., Moriconi, M. L., and Di Donfrancesco, G.: Differences in Arctic and Antarctic PSC occurrence as observed by lidar in Ny-Ålesund (79° N, 12° E) and McMurdo (78° S, 167° E), Atmos. Chem. Phys., 5, 2081–2090, doi:10.5194/acp-5-2081-2005, 2005.

McPeters, R. D., Labow, G. J., and Logan, J. A.: Ozone climatological profiles for satellite retrieval algorithms, J. Geophys. Res., 112, D05308, doi:10.1029/2005JD006823, 2007

Newman, P. A., Rex, M. (Lead Authors), Canziani, P. O., Carslaw, K. S., Drdla, K., Godin-Beekmann, S., Golden, D. M., Jackman, C. H., Kreher, K., Langematz, U., Müller, R., Nakane, H., Orsolini, Y. J., Salawitch, R. J., Santee, M. L., von Hobe, M., and Holden, S.: Polar Ozone: Past and Present, Chapter 4 in Scientific Assessment of Ozone Depletion: 2006, Global Ozone Research and Monitoring Project – Report No. 50. World Meteorological Organization, Geneva, Switzerland, 2007

Newman, P. A., Oman, L. D., Douglass, A. R., Fleming, E. L., Frith, S. M., Hurwitz, M. M., Kawa, S. R., Jackman, C. H., Krotkov, N. A., Nash, E. R., Nielsen, J. E., Pawson, S., Stolarski, R. S., and Velders, G. J. M.: What would have happened to the ozone layer if chlorofluorocarbons (CFCs) had not been regulated?, Atmos. Chem. Phys., 9, 2113–2128, doi:10.5194/acp-9-2113-2009, 2009.

Pommier, M., Law, K. S., Clerbaux, C., Turquety, S., Hurtmans, D., Hadji-Lazaro, J., Coheur, P.-F., Schlager, H., Ancellet, G., Paris, J.-D., Nédélec, P., Diskin, G. S., Podolske, J. R., Holloway, J. S., and Bernath, P.: IASI carbon monoxide validation over the Arctic during POLARCAT spring and summer campaigns, Atmos. Chem. Phys., 10, 10655–10678, doi:10.5194/acp-10-10655-2010, 2010.

Razavi, A., Clerbaux, C., Wespes, C., Clarisse, L., Hurtmans, D., Payan, S., Camy-Peyret, C., and Coheur, P. F.: Characterization of methane retrievals from the IASI space-borne sounder, Atmos. Chem. Phys., 9, 7889–7899, doi:10.5194/acp-9-7889-2009, 2009.

Razavi, A., Karagulian, F., Clarisse, L., Hurtmans, D., Coheur, P. F., Clerbaux, C., Müller, J. F., and Stavrakou, T.: Global distributions of methanol and formic acid retrieved for the first time from the IASI/MetOp thermal infrared sounder, Atmos. Chem. Phys., 11, 857–872, doi:10.5194/acp-11-857-2011, 2011.

Rodgers, C.: Inverse methods for atmospheric sounding : Theory and Practice, Series on Atmospheric, Oceanic and Planetary Physics – Vol. 2. World Scientific, New Jersey, London, Hong Kong, 2000.

Rothman, L. S., Jacquemart, D., Barbe, A., Benner, D. C., Birk, M., Brown, L. R., Carleer, M. R., Chackerian, C. Jr., Chance, K., Coudert, L. H., Dana, V., Devi, V. M., Flaud, J.-M., Gamache, R. R., Goldman, A., Hartman, J.-M., Jucks, K. W., Maki, A. G., Mandin, J.-Y., Massie, S. T., Orphal, J., Perrin, A., Rinsland, C. P., Smith, M. A. H., Tennyson, J., Tolchenov, R. N., Toth, R. A., Vander Auwera, J., Varanasi, P., and Wagner, G.: The HITRAN 2004 molecular spectroscopic database, J. Quant. Spectrosc. Ra., 96, 139–204, 2005.

Rothman, L. S., Gordon, I. E., Barbe, A., Benner, D. C., Bernath, P. F., Birk, M., Boudon, V., Brown, L. R., Campargue, A., Champion, J.-P., Chance, K., Coudert, L. H., Dana, V., Devi, V. M., Fally, S., Flaud, J.-M., Gamache, R. R., Goldman, A., Jacquemart, D., Kleiner, I., Lacome, N., Lafferty, W. J., Mandin, J.-Y., Massie, S. T., Mikhailenko, S. N., Miller, C. E., Moazzen-Ahmadi, N., Naumenko, O., Nikitin, A. V., Orphal, J., Perevalov, V. I., Perrin, A., Predoi-Cross, A., Rinsland, C. P., Rotger, M., Simecková, M., Smith, M. A. H., Sung, K., Tashkun, S. A., Tennyson, J., Toth, R. A., Vandaele, A. C., and Vander Auwera, J.: The HITRAN 2008 molecular spectroscopic database, J. Quant. Spectrosc. Ra., 110, 533–572, 2009.

Schneider, M., Redondas, A., Hase, F., Guirado, C., Blumenstock, T., and Cuevas, E.: Comparison of ground-based Brewer and FTIR total column O_3 monitoring techniques, Atmos. Chem. Phys., 8, 5535–5550, doi:10.5194/acp-8-5535-2008, 2008.

Slaper, H., Velders, G. J. M., Daniel, J. S., DeGruijil, F. R., and Van der Leun, J. C.: Estimates of ozone depletion and skin cancer incidence to examine the Vienna Convention achievements, Nature 384, 256–258, 1996

SPARC CCMVal: SPARC Report on the Evaluation of Chemistry-Climate Models, edited by: Eyring, V., Shepherd, T. G., and Waugh, D. W., SPARC Report No. 5, WCRP-132, WMO/TD-No. 1526, available at: http://www.atmosp.physics.utoronto.ca/SPARC, 2010.

Turquety, S., Hadji-Lazaro, J., Clerbaux, C., Hauglustaine, D., Clough, S. A., Cassé, V., and Schlüssel, P.: Operational trace gas retrieval algorithm for the Infrared Atmospheric Sounding Interferometer, J. Geophys. Res., 109, D21301, doi:10.1029/2004JD004821, 2004.

van der A, R. J., Allaart, M. A. F., and Eskes, H. J.: Multi sensor reanalysis of total ozone, Atmos. Chem. Phys., 10, 11277–11294, doi:10.5194/acp-10-11277-2010, 2010.

van Roozendael, M., Loyola, D., Spurr, R., Balis, D., Lambert, J. C., Livschitz, Y. , Valks, P., Ruppert, T., Kenter, P., Fayt, C., and Zehner, C.: Ten years of GOME/ERS2 total ozone data: the new GOME data processor (GDP) version 4: I.Algorithm description, J. Geophys. Res., 111, D14311, doi:10/1029/2005JD006375, 2006

von Savigny, C., Rozanov, A., Bovensmann, H., Eichmann, K.-U., Noel, S., Rozanov, V. V., Sinnhuber, B.-M.,Weber, M., Burrows, J. P., and Kaiser, J. W.: The ozone hole break-up in September 2002 as seen by SCIAMACHY on ENVISAT, J. Atmos. Sci., 62, 721–734, doi:10.1175/JAS-3328.1, 2005.

Wan, Z.: New refinements and validation of the MODIS land surface temperature/emissivity products, Remote Sens. Environ., 512, 59–74, 2008

Weber, M., Dhomse, S., Wittrock, F., Richter, A., Sinnhuber, B.-M., and Burrows, J. P.: Dynamical Control of NH and SH Winter/Spring Total Ozone from GOME Observations in 1995-2002 Geophys. Res. Lett, 30, 1853, doi:10.1029/2002GL016799, 2003.

Wespes, C., Hurtmans, D., Clerbaux, C., Santee, M. L., Martin,

R. V., and Coheur, P. F.: Global distributions of nitric acid from IASI/MetOP measurements, Atmos. Chem. Phys., 9, 7949–7962, doi:10.5194/acp-9-7949-2009, 2009.

Worden, J., Liu, X., Bowman, K., Chance, K., Beer, R., Eldering, A., Gunson, M., and Worden, H.: Improved tropospheric ozone profile retrievals using OMI and TES radiances, Geophys. Res. Lett., 34, L01809, doi:10.1029/2006GL027806, 2007.

World Meteorological Organization (WMO): Scientific assessment of ozone depletion, Global ozone and research and monitoring project, Report No. 47, Geneva, Switzeland, 2002

World Meteorological Organization (WMO): Scientific assessment of ozone depletion, Global ozone and research and monitoring project, Report No. 52, Geneva, Switzeland, 2010

Zhang, L., Jacob, D. J., Liu, X., Logan, J. A., Chance, K., Eldering, A., and Bojkov, B. R.: Intercomparison methods for satellite measurements of atmospheric composition: application to tropospheric ozone from TES and OMI, Atmos. Chem. Phys., 10, 4725–4739, doi:10.5194/acp-10-4725-2010, 2010.